Materials Science and Engineering C 50 (2015) 85–96

Contents lists available at ScienceDirect

Materials Science and Engineering C

journal homepage: www.elsevier.com/locate/msec

Finite element analysis of stress distributions in mono- and bi-cortical dental implants

F. Lofaj [a,b], J. Kučera [c], D. Németh [a,*], L. Kvetková [a]

[a] Institute of Materials Research of Slovak Academy of Sciences, Watsonova 47, 04001 Košice, Slovak Republic
[b] Faculty of Materials Science and Technology in Trnava, Slovak University of Technology in Bratislava, 916 24 Trnava, Slovak Republic
[c] Stonek, s.r.o., Krivá 23, 040 01 Košice, Slovak Republic

ARTICLE INFO

Article history:
Received 29 October 2014
Received in revised form 23 December 2014
Accepted 30 January 2015
Available online 2 February 2015

Keywords:
Dental implants
Cortical bone
Monocortical fixation
Bicortical fixation
FEA stress distribution

ABSTRACT

The finite element analysis (FEA) of the stress distribution in the mono- and bicortically fixed implants subjected to 3-axial loading was performed and verified experimentally on a model mandible to evaluate the benefits of each type of fixation from the viewpoint of the compressive stress reduction in the cortical part of atrophied mandible. The analysis revealed that the highest compressive stresses in the cortical bone are generated at the edge of the cortical bone where the highest torque from the implant is acting. The most effective way to reduce the maximum level of compressive stresses in the cortical bone and in the implant is the recession of the implant thread slightly below the surface of the cortical bone. Shortening of the intraosseal length of the implant and/or thinning of the upper cortical bone result in a substantial increase of the maximum compressive stresses. The comparison of FEA and model experiments suggests that bicortical fixation is the most efficient in the fresh implants and the advantage of bicortical fixation compared to monocortical fixation decreases with time due to osteointegration, possibly as a result of gradual suppression of sliding between the bone and implant during loading.

© 2015 Elsevier B.V. All rights reserved.

1. Introduction

The replacement of lost teeth by dental implants in the mandible became a common technique to this esthetical and health problem during the last decade. For healthy jawbones with sufficient height and width, conventional two-phase metallic dental implants with the diameter more than 3.5 mm are used. Such implants were introduced in the mid-1960s after Brånemark demonstrated the possibility of osteointegration — structural integration of a biocompatible metal into the living bone at biochemical level [1]. Later it was found out that the changes of shape, length and width of implants could influence the level of the implant osteointegration. The application of this theory to dental implants reduced the dependence on mechanical interlocking and enabled the development of implant systems in more versatile enosseous design [2–4]. However, the application of dental implants in the anterior part of the mandible still remains a challenging task. This is because massive atrophic changes often occur after teeth removal and due to aging which result in significant reduction of the vertical and horizontal dimensions of the mandible as well as in the loss of bone density. The level of atrophy is classified based on the size changes according to Lekholm and Zarb classification [5]. The classification of Cawood and Howell [6] is also frequently cited. They showed that the average heights of the highly atrophied mandibles may be reduced down to 21.3–12.7 mm, and the corresponding widths to 15–10 mm, respectively. Different ways to classify the atrophy is based on the absolute bone volume index (ABV) which is a ratio of the trabecular bone volume to total bone volume. According to Bodic et al. [7], ABV ratio in the healthy mandible is 50.2 ± 11.8%. It decreases with age to 30–50% in male population and to 22–30% in female population.

Obviously, conventional two phase dental implants with large diameter cannot be fixed in such thin and low atrophied bones. The implants have to be single phase to have smaller diameter and their length must be adjusted to the bone profile. A new class of single phase implants has therefore developed for these cases. They have a shape of a thin screw with various thread pitch and width. The neck diameter is usually less than 2.25 mm and their length varies depending on the height of the mandible. It may also have three notches near the tip for better osteointegration with the bone. The implants can be fixed in the bone either only in the upper cortical bone or in both upper and lower cortical bones. The first case, when the implant tip is "free" in the trabecular bone, is called monocortical fixation. In the second case called bicortical fixation, implant neck is fixed in the upper cortical bone and its tip is embedded into the lower cortical bone.

Monocortical fixation is commonly used in the case of healthy and even atrophied bones [8]. However, bicortical type of fixations is expected to increase the resistance of bone against vertical load [9]. This is critical especially in highly atrophied mandibles when both the bone

* Corresponding author.
E-mail address: dusan.nemeth23@gmail.com (D. Németh).

http://dx.doi.org/10.1016/j.msec.2015.01.095
0928-4931/© 2015 Elsevier B.V. All rights reserved.

and implant are subjected to wide range of occlusal and masticatory forces [10,11]. If the related stresses exceed the strength of the bone or implant, their failure may occur [12,13]. To prevent that, the reduction of maximum stresses well below the bone strength is required. Obviously, the calculation of stress and deformation distributions in the implant and adjacent bone are necessary for the design of the implants. The development of a single mathematical model is difficult due to geometry, material and bond system complexity. Therefore, sophisticated mathematical simulations such as finite element analysis (FEA) were introduced to visualize the corresponding distributions [14,15].

FEA is able to calculate stress distributions in cortical and spongious part of mandible for various implants, fixations and bone geometry. FEA was often used on conventional and monocortical screw implants in monocortical fixation and a number of authors demonstrated that the stresses generated by the vertical occlusal forces are concentrated in the neck of the implant and in the surrounding cortical bone [14,15]. Interestingly, the bicortical fixation of thin, screw type implants in atrophied mandible is studied considerably less than the monocortical fixation. Among few, Pierrisnard in his FEA study evaluated stress distributions in the implants with different lengths [16]. It was found out that regardless of the length of the implant, the stresses generated in the implant with bicortical fixation were slightly higher than in monocortical fixation. Ivanoff et al. [2] also reported up to four times more frequent failures of bicortical screws compared to monocortical implants due to enhanced non-axial forces in the neck zone of the implant. These results seem to be contradictory to the general expectation that bicortical fixation generates lower stresses in the upper cortical bone due to additional support of the implant tip. Therefore, the aim of this work is to compare the stress distributions in cortical and trabecular parts of the model mandible by FEM analysis using linear static methods for monocortical and bicortical fixation of dental implant subjected to 3-axial loading and to verify it experimentally on model mandible. The comparison is focused on the implant neck zone and on the evaluation of the influence of the position of neck of implant with regard to the surface of the cortical bone. The results of FEA are compared with the measurement of "yield strength" of the model bone and real implant under corresponding 3-axial loading.

2. Experimental procedure

2.1. Mandible model

Depending on the atrophy level, mandibles exhibit significant variations of their shape and size [5–7] which cannot be accommodated in single FEA calculation. However, the shape of the mandible is of lesser importance because the maximum forces are always concentrated in the small localized zones in the neck of the implant and in the adjacent cortical bone [15,16]. The dimensions and the properties of the cortical bone are the crucial parameters. Thus, the FEA calculations can be performed on model mandibles with any reasonable shape but with variable height, thickness of the cortical bone and ABV ratio.

To obtain the size data of the corresponding parameters, 178 CT scans of edentulous atrophic mandibles were evaluated. The group consisted of 84 men (age interval 52–72 years) and 94 women (age interval 48–68 years). The frontal part of the mandible in the canine region and in the mental foramina, where the greatest atrophic changes are observed, was analyzed. The height and width of the contours of CT cross sections (Fig. 1) were classified according to Cawood and Howell [6]. In the men's group, the atrophy was from levels III to V, in the women's group from levels IV to VI. In the men's group, the corresponding mandible height range was from 26.8 mm down to 11.3 mm (with the mean value of 19.3 mm) and width from 14.8 mm to 10.1 mm (mean value 11.2 mm). In the women's group, the height range was from 21.1 mm to 9.8 mm (mean value 16.8 mm and width from 13.9 mm to 8.5 mm) (mean value 10.8 mm). The thickness of

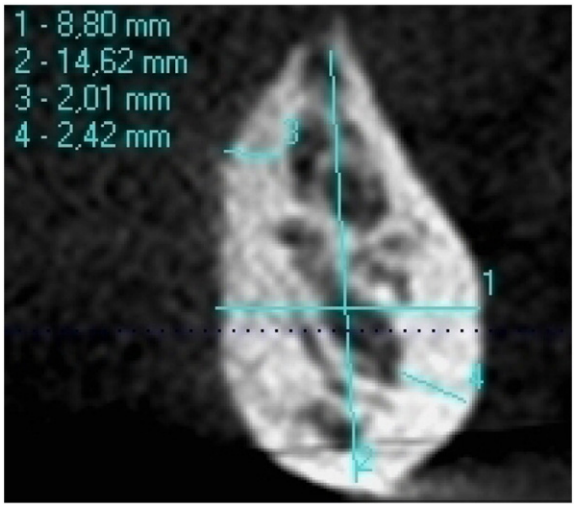

Fig. 1. Typical CT cross section of the atrophied mandible in the zone of mental foramina to illustrate the variations in the cortical bone thickness and density. The measured values include: 1 — width and 2 — height of the jaw, 3 and 4 — width of the cortical bone in different areas.

cortical bone in the crestal region ranged from 0.2 mm to 2.5 mm and from 0.5 mm to 4.9 mm in the bottom part of the mandible. The ABV index in the men's group was in the range 52–33% and in the women's group 78–36%. These data were used as the variables for the model of the atrophied mandible.

The shape of the simplified model of the mandible in the form of trapezoid has been selected for FEA calculations (Fig. 2). The variables included two different heights, 17.5 mm (Fig. 2a and b) and 12 mm (Fig. 2c and d), corresponding to the atrophied and highly atrophied jawbones with different ABV while keeping the length of the intraosseal part of the implant constant (14 mm and 8.5 mm, respectively). To obtain mono- and bicortical fixations, the thickness of the bottom cortical bone has been adjusted accordingly.

Besides implant length and bone height, three different positions of the implant thread with regard to the position of upper cortical bone were considered: the beginning of the thread is located 0.5 mm below the surface (as indicated in Fig. 2), the recess is only 0.2 mm below the surface, or the implant is not fully recessed and the beginning of the thread is located 0.5 mm above the bone surface. The last case may occur after certain time due to continuous bone atrophy.

Two certified (CE 1293.40042/101/1/2009/CE (ISO9001)) commercial implants designated as SVMB 3.0–14 D and SVMB 3.0–8.5 D (Martikan, Slovak Republic) were used for both FEA and experimental measurements (Fig. 3a). These implants with small diameter were primarily developed for the indications in frontal part of atrophied mandible for bi- and mono-cortical fixations [17]. They were identical, just the lengths of the intraosseal part (thread) in the implants were 14 mm and 8.5 mm, respectively. The thread diameter and inner diameter of the implant were 3.0 mm and 2.0 mm, respectively. The original three dimensional model of the implant in the ProEngineer software has been imported into the SolidWorks. The geometry of the implant was used to create thread in the adjacent cortical and spongious bones using Boolean operations.

2.2. Finite element analysis (FEA)

Geometrical boundary conditions used in the analysis simulated strong fixation of the model segment of the mandible in the remaining body of the mandible (Fig. 3a). Physical boundary conditions defined the loading point in such a way that it was always at the distance of 28.7 mm from the bottom of the mandible regardless of its height and implant fixation (Fig. 3a). This distance corresponds to the case of a

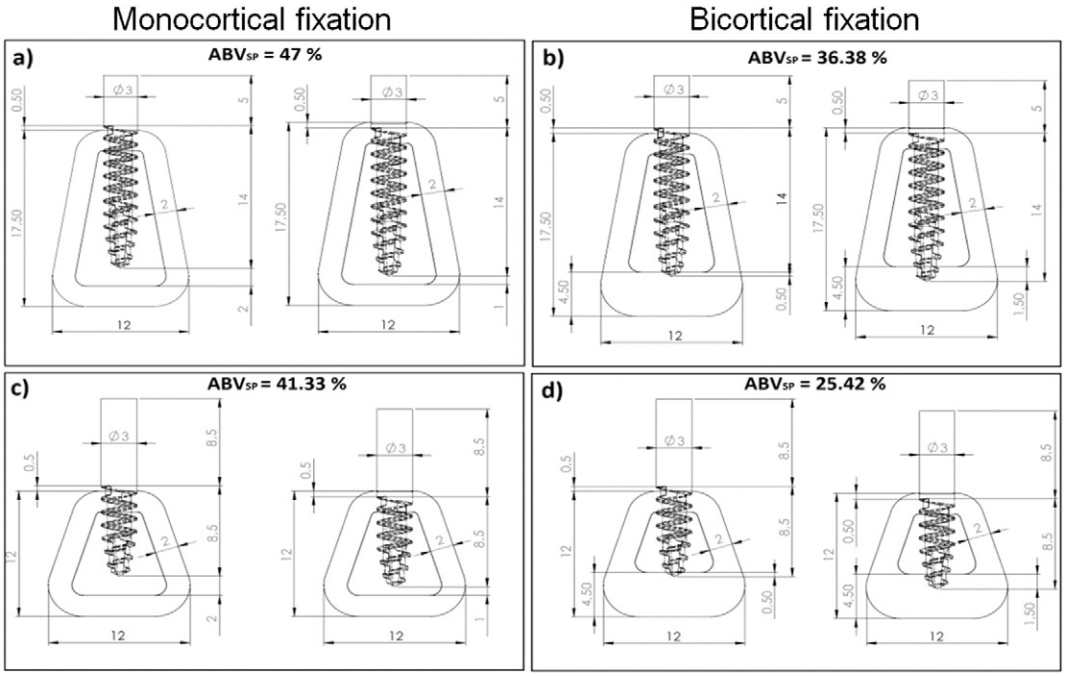

Fig. 2. The geometry and dimensions of the model jawbone and real implant in the cases of its mono- and bicortical fixation for atrophied mandible with the height of 17.5 mm — a), b) and highly atrophied bone with the height of only 12 mm — c), d). The length of the intraosseal part of the implant was constant, 14 mm and 8.5 mm, respectively, and the thickness of the bottom corticalis has been adjusted according to the fixation modeled. The implant thread is located 0.5 mm below the surface of the upper cortical bone.

healthy tooth in the mandible. In the case of tooth replacement, this distance is adjusted by the size of the crown on the implant [18,19]. The use of one loading point at the selected distance is justified by the fact that any number of complex forces on the crown can be replaced by one vector sum of these forces which consists of three main components in x, y and z directions. In the general case, the resulting force consisting from the loads applied in all three main directions has been considered because pure occlusal forces are not common. Adapted from the work of Mericske-Stern et al. [20], vertical (normal) force of $F_y = 114.6$ N, mesiodistal force of $F_z = 23.4$ N and vestibulolingual force of $F_x = 17.1$ N were used for the calculations. These main components summarize into overall resulting force of 118 N.

The tetrahedron elements with different sizes were used for the mesh in the implant and bone (Fig. 3 b). The mesh size in the regions of interest with the maximum stresses was determined automatically based on convergence using h-method and assuming the limit for the total strain energy error of 2%. As indicated in Fig. 4, the accuracy level for the total relative strain energy error of 1.98% was reached. The corresponding mesh size has been around 0.2 mm. The total number of elements was 1,052,610 and the number of nodes was 1,439,586.

The purpose of the calculations was to visualize stress distributions in the implant, cortical and trabecular bone and to determine the maximum stresses to reveal the critical points of the implant–bone system. The analysis has been intentionally limited to linear-elastic region because the level of masticatory forces has to be well below the level of the yield stresses of the bone and implant to avoid their damage. Therefore, linear static finite element analysis is sufficient to calculate stress distributions in the implant, cortical and spongious bone. FEA has been performed in SolidWorks software for 24 cases covering the atrophy range observed in CT including two mandible heights and three implant positions for both monocortical and bicortical fixations. The elastic properties used for the calculation are summarized in Table 1 [21,22]. Possible anisotropy of the elastic properties as well as variations in bone density were not considered because of lack of reliable data, simplification for the understanding and to keep the number of calculations reasonable.

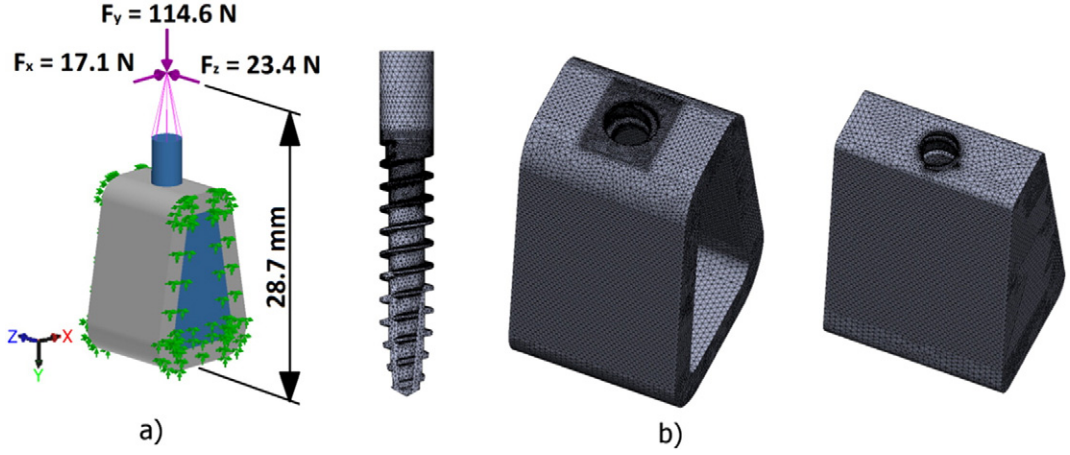

Fig. 3. Geometrical and physical boundary conditions a) and the geometry of the implant and the mesh of finite elements in the cortical and trabecular bone b).

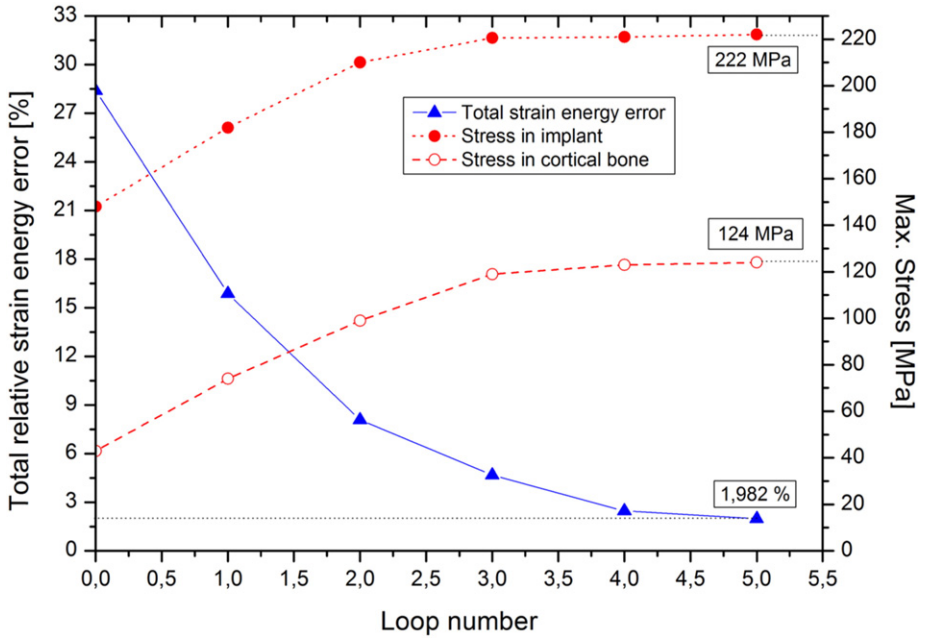

Fig. 4. Iterative determination of the maximum von Mises stresses using the h-adaptive method for 2% total strain energy error.

2.3. Mechanical testing

The mandible for the experimental investigations of the above mentioned implants during loading was modeled by the composite wooden bars with rectangular cross section. The difference between trapezoidal and rectangular shape was considered unimportant because the stresses are always concentrated in the zone close to the implant. The bars consisted of dense tough ash wood top layer glued on the soft porous balsa wood core from each side. Balsa and ash wood were reported to have elastic properties close to those of cortical and trabecular bone, respectively, and the such wooden composites have already been used to model mechanical behavior of the human bone [22]. As indicated in Table 1, the tabulated elastic properties of ash wood are really close to that of cortical bone. Young's modulus of balsa is only half of that in trabecular bone but it is considered to be acceptable for the case of experimental comparison because it is not the main load bearing part. The width of the bars was constant (12 mm). The height of the composite bars was 11.5 mm, 13.5 mm, 15.5 mm and 17.5 mm and the thickness of the ash wood rim was 2 mm and 2.5 mm, respectively, to obtain different levels of atrophy via height and ABV changes (Table 2). Because the lengths of the available implants were only 14.5 mm and 8.5 mm, monocortical fixation was possible only in the bars with the height of 15.5 mm and 17.5 mm.

To fix each implant in the bar, the holes with the diameter corresponding to the inner diameter of each implant were pre-drilled into the wooden bars. The implants were screwed into the model bone using 50 Nm torque either in monocortical or bicortical fixation depending on the size of the wooden block. This torque resulted in slightly recessed position of the implant which corresponds approximately to the FEA case with 0.2 mm recessed thread. The other thread position cases were not tested because of uncertainty with their adjustment and reproducibility.

The compressive tests were performed on an LR5K Plus (Lloyd, UK) testing machine with the bone–implant system fixed in a specially designed fixture (see Fig. 5). The load from the crosshead was applied normally to the loading rod with the crosshead speed of 0.05 mm/min. However, the contact plane of the loading rod and implant was tilted (81.5° in x direction and 78.5° in y direction) in two directions in such a way that the ratio $F_x/F_y/F_z$ was equal to the ratio used for FEA calculation. The distance of the loading point from the bone of 28.7 mm was adjusted by a spacer screwed on the implant.

The experiments were performed in such a way that the force was increased until the apparent ultimate strength was achieved and then intentionally stopped to prevent damage of the implant. The force corresponding to the yield point was determined from the force–extension curves for each test. At least 3 valid tests were performed for each implant and for both fixations.

3. Results

3.1. FEA stress distribution in the implant

The overall stress distribution in the implants with 14 mm intraosseal length in monocortical fixation obtained by FEA is shown in Fig. 6 on a cross section of the implant/bone system. The plane of the cross section is tilted to pass through the maximum stresses. Such distribution was

Table 1
Elastic properties of the implant, cortical and trabecular bone for FEA calculations and the corresponding properties of ash wood and balsa used to mimic the bone in the model material [21,22].

	Bone		Wood materials		Metallic material
	Cortical bone	Trabecular bone	Ash wood	Balsa	Implant Ti–Al6–V4 Gr.5
Elastic modulus E [GPa]	13.7	2.3	15.7	1.2	114
Poisson's ratio μ [−]	0.3	0.3	0.3	0.3	0.3
Yield stress R_p [MPa]	–	–	–	–	825

Table 2
The dimensions of the model bones and implants used for mechanical testing.

No.	Height of modeled bone [mm]	Thickness of ash wood (cortical bone) [mm]	Implant length [mm]	Fixation	Absolute "bone" volume ABV [%]
1	17.5	2	14	Monocortical	51
2	15.5	2	14	Bicortical	49
3	13.5	2	8.5	Monocortical	47
4	11.5	2	8.5	Bicortical	43
5	17.5	2.5	14	Monocortical	41
6	15.5	2.5	14	Bicortical	39
7	13.5	2.5	8.5	Monocortical	37
8	11.5	2.5	8.5	Bicortical	33

typical for each type of fixation and implant position; the differences were only in the absolute values of the maximum stresses. The level of the elastic deformation in Fig. 6 is intentionally magnified 140 times to make the deformation of the whole system visible (true deformation is shown as a shadow for comparison). Obviously, 3-axial loading caused not only compression deformation but also bending deformation of the implant and bone as well. The bending of the implant occurred as if it was compressed with larger force at the left side than at the right side of the implant. This approximation allows us easier understanding of the deformation of the adjacent bone: its both sides are depressed in comparison with the original bone surface but the right side is depressed more than the left side. Therefore, it appears to be lifted compared to the bone level on the left side of the implant.

The stresses are visualized on the cross section by different colors and the blue color corresponds to the stresses below 40 MPa, green color to around 100 MPa and red to the stresses above 200 MPa. Red color indicates that the highest stresses concentrated at approximately 5 different locations marked by numbers. The highest stresses (1i) developed at the bottom root of the implant head on the left side which is under the highest compressive stresses. The second highest stress concentrator (2i) is at the bone surface where the implant is compressed the most. The other stress concentrators were at the bended side of the implant. The (3i) stress concentrator was again at the root of the bottom side of the implant head followed by the stress zone at the surface (4i). The lowest stresses among the concentrators were found out at the root of the first thread (5i). The occurrence of this concentrator depended on the implant position in the upper cortical bone, respectively on the mutual position of that thread and cortical bone.

Detail 3D visualization of the principal stresses for the nodes in the zones with the highest stresses is in Fig. 7. It indicates the stress concentrators in five zones seen in Fig. 6. The inserts show not only the magnitude of the maximum von Mises (reduced) stresses, σ_{vM}, for each concentrator, but also the principal stresses σ_1, σ_2 and σ_3 along the corresponding directions P1, P2 and P3. The relationship among the principal stresses and von Mises stress is given by the formula [23].

$$\sigma_{vM} = \sqrt{\sigma_1^2 + \sigma_2^2 + \sigma_3^2 - (\sigma_1 \cdot \sigma_2 + \sigma_1 \cdot \sigma_3 + \sigma_2 \cdot \sigma_3)}.$$

Fig. 5. The model bone in the fixture and loading in the testing machine.

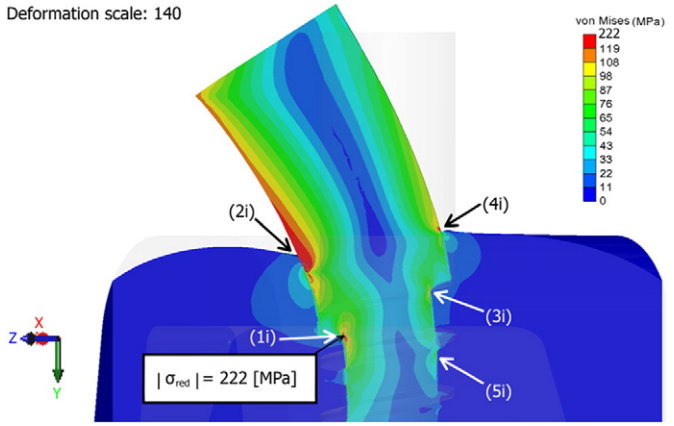

Fig. 6. The cross section of the implant and the bone with the stress distribution visualized by FEA. The case corresponds to the monocortically fixed 14 mm long implant with the thread screwed 0.5 mm below the surface of the cortical bone. The stress concentration zones are numbered from (1i) through (5i), where the highest stresses are in (1i) and index "i" relates to the implant.

Obviously, this formula cannot distinguish between tensile and compressive stresses. However, the inserts indicate that both, tensile and compressive stress components were present depending on the location. In the zone (1i) with the maximum of $\sigma_{vM} = 222$ MPa, the principal stress components σ_2 and σ_3 were compressive and σ_1 in P1 direction was tensile. The highest von Mises stress in the zone (2i) consisted only of compressive principal stresses whereas tensile stresses were dominant on the opposite side of the implant in the zones (3i)–(5i). However, von Mises stresses were always the highest in the zones (1i) and (2i) and therefore, the attention is further focused only on these two zones.

The position of the implant thread with regard to the bone surface had a profound effect of the magnitude of von Mises stresses and even on the location of the zone with the stress concentration. Figs. 8 and 9 illustrate these effects for monocortical and bicortical fixations, respectively, and three positions of the thread. The changes were the strongest when the implant thread beginning was located 0.5 mm above the cortical bone surface (Figs. 8a and 9a). The maximum stresses were higher than 415 MPa in the zone (1i) whereas the stresses in the zone (2i) were only 327 MPa and 236 MPa, respectively. Moreover, zones (1i) and (2i) exchanged their position in comparison with their position in the case in Fig. 7. Dramatical increase of von Mises stress in the insufficiently screwed implant seems to result from its reduced cross section among threads. When the implant was screwed deeper into the cortical bone (Figs. 8b–c and 9b–c), the differences between the magnitude of the von Mises stresses became only 9–10% and 7.6% for the positions 0.2 mm and 0.5 mm below the bone surface, respectively. Stresses were slightly lower in the bicortical case but the differences were insignificant. The corresponding principal and von Mises stresses in the (1i) zones are summarized in Table 3.

3.2. FEA stress distribution in the bone

Stress distributions in the cortical bone were analyzed in the same way as in the implant. Fig. 10 visualizes the stresses in the half of the cortical bone. The stresses concentrated in the zones which were adjacent to the stress concentrators in the implant. However, several differences can be observed. First, the stress levels in the cortical bone were significantly lower than in the implant. The highest von Mises stresses were at the upper edge of the bone which was not adjacent to the zone (1i) but to the zone (2i) in the implant. Three stress concentrators were on the "compressive" side while only two of them were on the "tensile" side. It is opposite to the distribution of the concentrators in the implant (compare Figs. 7 and 11).

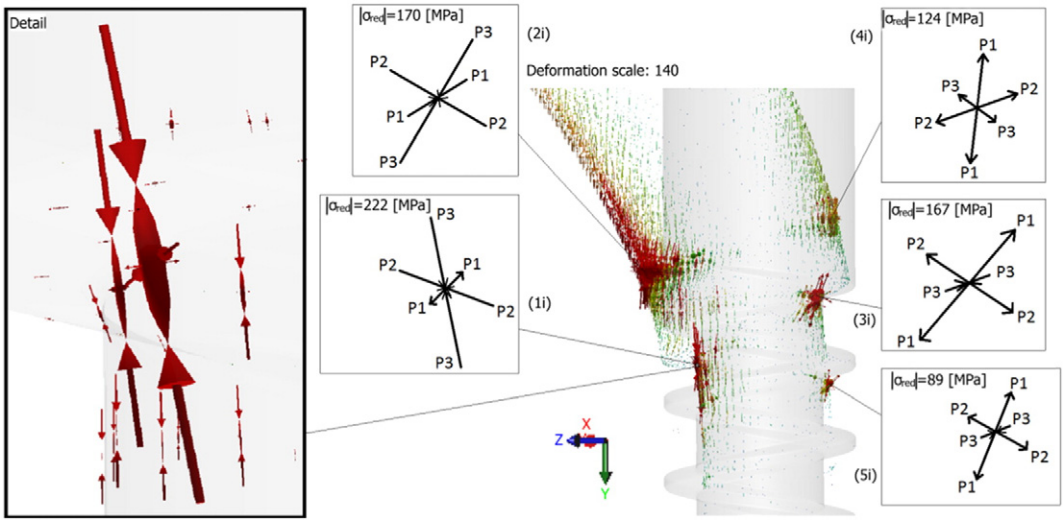

Fig. 7. The 3-D visualization of the distribution of principal stresses in the implant and in the case corresponding to Fig. 6. The inserts in zones with the highest reduced stresses show the principal stresses in three main directions and which result in the indicated reduced stress.

Fig. 11 illustrates the locations of the zones with stress concentration in the cortical bone intentionally magnified 140 times to facilitate the understanding of the correlation between stress and deformation. The principal stresses in the zone (2b) were only tensile, the zone opposite to it consisted of only compressive components and the other stresses contained both compressive and tensile components (see also Table 3).

The effects of the fixation and implant position are summarized in Fig. 12. The comparison was easier than in the implant, because the highest stresses remained always at the upper edge, which is marked as zone (1b). Extremely high von Mises stresses (346 MPa and 367 MPa in bi- and monocortical fixation, respectively) were generated in the zone (2b) when the implant has been insufficiently screwed into the bone. The values of σ_{vM} in the zone (1b) were dramatically reduced to 155–120 MPa when implant was screwed deeper into the bone (−0.2 mm and −0.5 mm). The stresses in the other stress concentration zones (3b)–(5b) were even lower. The general tendency was stress decrease with deeper position of the implant and the monocortical fixation resulted in slightly higher stress than in the bicortical case. The level of stresses in the trabecular bone has been more than one order of magnitude lower than those in the cortical bone.

Obviously, the zone (1b) with the highest stresses in the cortical bone is the most critical and the other zones may be neglected. The principal stresses and von Mises stresses in zone (1b) for two intraosseal lengths in the cortical and trabecular bone are compared in Table 3 with the analogous stresses in the implant. The corresponding values of von Mises stress in zone (1b) in the implant and in the cortical bone are plotted in relative units in Fig. 13.

The differences in σ_{vM} in the zone (1i) in the implant and in the zone (1b) in the cortical bone between the fixations were quite small, usually within 1–2% of the corresponding maximum value. Thus, the advantage of bicortical fixation in generating lower stresses is almost negligible. The intraosseal length decrease from 14 mm to 8.5 mm resulted in the increase of σ_{vM} by 36%–65% in the monocortically fixed implant and by 37–63% in the bicortical case depending of the thread position. The corresponding ranges in the cortical bone were 54–70% and 40–50%. However, much stronger changes of the maximum stress were seen when the implant was screwed deeper into the bone. Assuming the maximum stresses in the implant position 0.2 mm below the bone surface level to be 100%, the maximum relative von Mises stresses in the case +0.5 mm above the bone surface corresponded to ~215% in the case of 8.5 mm (intraosseal length) monocortical implant and ~179% in 14 mm implant. The values for bicortical fixation were only slightly lower. When the implant was screwed 0.5 mm below the bone surface, the maximum relative stresses were 3–6% lower in comparison with 0.2 mm position depending on the implant length and fixation.

3.3. Mechanical testing

Fig. 14 shows typical load–displacement curves obtained from compressive tests with 3-axial loading. The curve consists of linear part until the load marked as F_p and then its slope declines until maximum is reached at the load F_m. The values of F_p and F_m are principally related to the yield strength, R_p, and to the strength of the studied material, R_m, respectively. However, because of unknown cross sections to which those critical loads can be related, calculation of the corresponding stresses from the measured loads is not possible and only the "yield" load and "strength" force values were used for relative comparison and for the comparison with the FEA results. Fig. 14 also illustrates the influence of mono- and bicortical fixation on load–

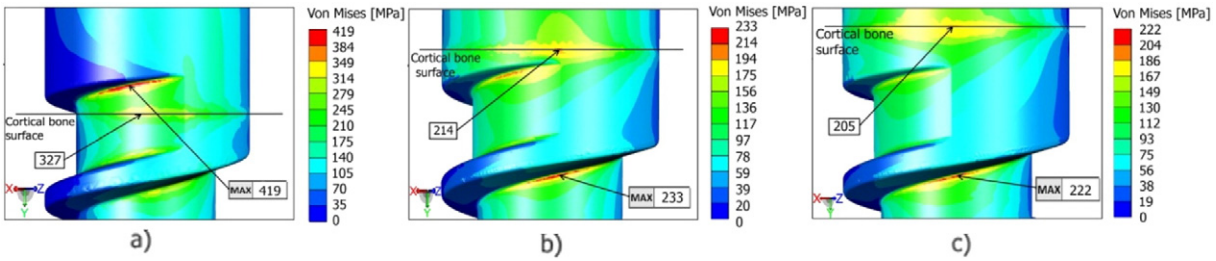

Fig. 8. The maximum stresses in the implants with 14 mm intraosseal length in the case of monocortical fixation and three positions of the thread beginning: a) − 0.5 mm above, b) − 0.2 mm below and c) − 0.5 mm below the surface.

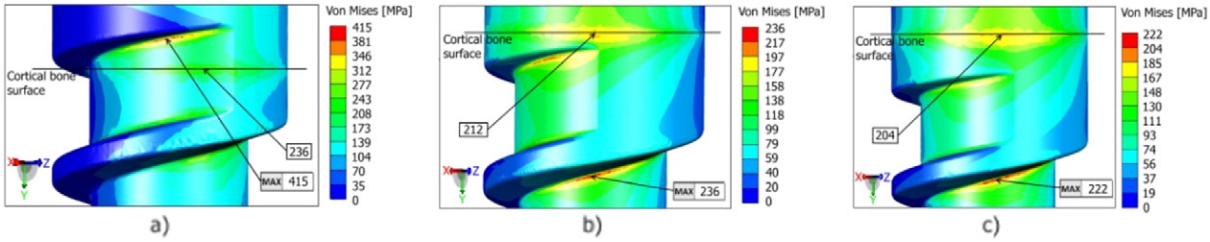

Fig. 9. The maximum stresses in the implants in the case of bicortical fixation and three positions: a) — 0.5 mm above, b) — 0.2 mm below and c) — 0.5 mm below the surface.

displacement curves in the same model bone. The slopes of the linear part of the curves as well as the values obtained in the monocortical fixation were different, but the F_p and especially F_m values in monocortical fixation were always lower than in bicortical case.

Fig. 15 compares the curves depending on the fixation and intraosseal length of the implant in two model bones with two different thickness of "cortical bone". The corresponding forces F_p and F_m values are summarized in Table 4 and in Fig. 16 as a function of intraosseal length, bone thickness and even ABV index for easier comparison. The conclusions are that bicortical fixation of longer implant in thicker "cortical" bone results in the highest yield and strength forces of the whole bone/implant system. ABV index does not seem to be a relevant parameter because of the localization of maximum stresses.

4. Discussion

The current FEA calculations assumed strong bond among the implant and bone. It corresponded to fully osteointegrated implant. However, the freshly introduced implant can have only a weak interface. This case was not modeled and this limitation has to be considered during interpretation of the current data.

Figs. 6–7 and 10–11 indicated the existence of several stress concentrators which were different in the implant and in the adjacent cortical bone. Moreover, the resulting von Mises stresses were composed of different principal stresses — only compressive stresses were present in the "compressed" side of the implant and cortical bone, but tensile components were on the opposite side. The concentrators at the threads had usually both types of principal stresses. Although the tensile stresses are required for the crack initiation and propagation in the inorganic materials, compressive stresses in the living bones are more dangerous because they cause bone recession, thinning and atrophy, which ultimately result in bone failure when the local stresses exceed the bone strength. In contrary, small tensile stresses activate bone growth and result in stress decrease. Thus, the attention has to be focused on the areas with the highest compressive stresses in the load-bearing cortical bone, i.e. on the zone (1b) in Figs. 10 and in 11, which are located close to the zone (2i) in the implant.

Table 3
The maximum reduced stresses and the corresponding principal stresses in the implant, cortical and trabecular bone in the cases of two types of implant fixation, two intraosseal lengths of the implant and three positions of the implant thread with regard to the surface of the cortical bone.

Intraosseal implant length								
8.5 mm					14 mm			
Thread position [mm]	Principal stress [MPa]			Reduced stress [MPa]	Principal stress [MPa]			Reduced stress [MPa]
	σ_1	σ_2	σ_3	σ_{red}	σ_1	σ_2	σ_3	σ_{red}
				Implant				
				Monocortical fixation				
−0.5	−56	−167	−795	690	−31	−110	−484	419
−0.2	4	−39	−336	321	2	−21	−242	233
−0.5	2	−40	−318	301	1	−24	−233	222
				Bicortical fixation				
−0,5	−34	−155	−766	679	−27	−118	−480	415
−0,2	0	−33	−243	328	1	−23	−246	236
−0,5	2	−35	−320	305	1	−24	−232	222
				Cortical bone				
				Monocortical fixation				
−0.5	−932	−388	−305	590	−521	−182	−169	346
−0.2	−144	−233	−395	221	−102	−176	−279	154
−0.5	−133	−220	−353	191	−90	−156	−233	124
				Bicortical fixation				
−0.5	−992	−440	−328	616	−532	−172	−157	367
−0.2	−143	−227	−374	203	−81	−124	−232	135
−0.5	−110	−200	−306	170	−88	−150	−228	121
				Trabecular bone				
				Monocortical fixation				
−0.5	12	5	−4	14	10	−6	−3	11
−0.2	18	9	−2	17	6	−5	−4	9
−0.5	12	3	−5	15	7	−2	−3	10
				Bicortical fixation				
−0.5	10	6	−5	13	5	−2	−6	10
−0.2	13	6	−5	16	6	−3	−5	10
−0.5	14	4	−5	16	7	−2	−3	10

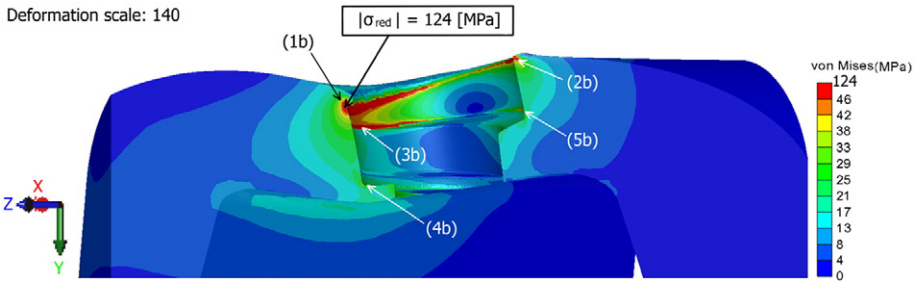

Fig. 10. Detail visualization of the stress distribution in the cortical bone adjacent to the implant. The case corresponds to Fig. 6 but the implant is hidden and stress range adjusted.

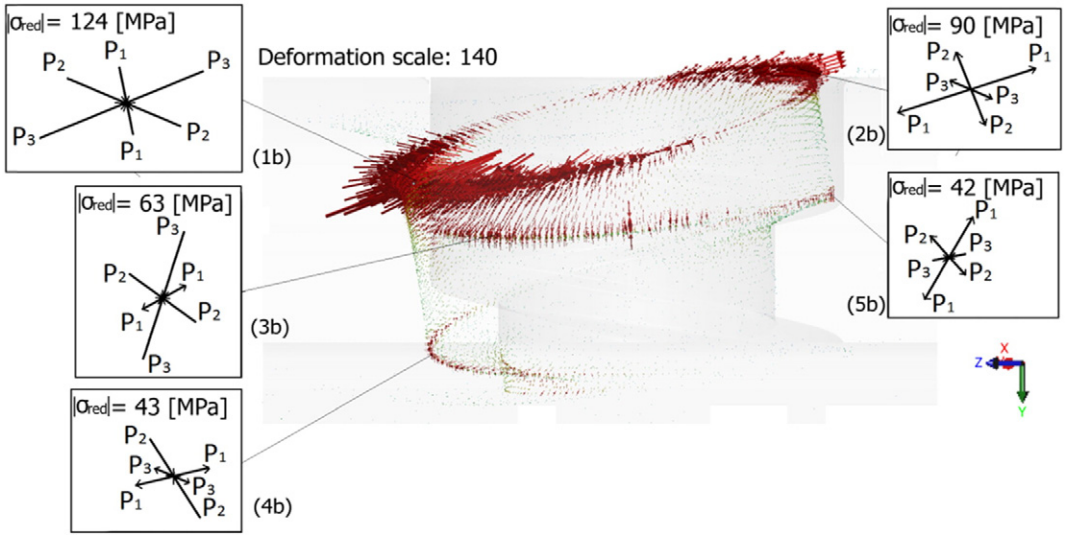

Fig. 11. The distribution of the principal stresses in the cortical bone adjacent to the implant shown in Fig. 10.

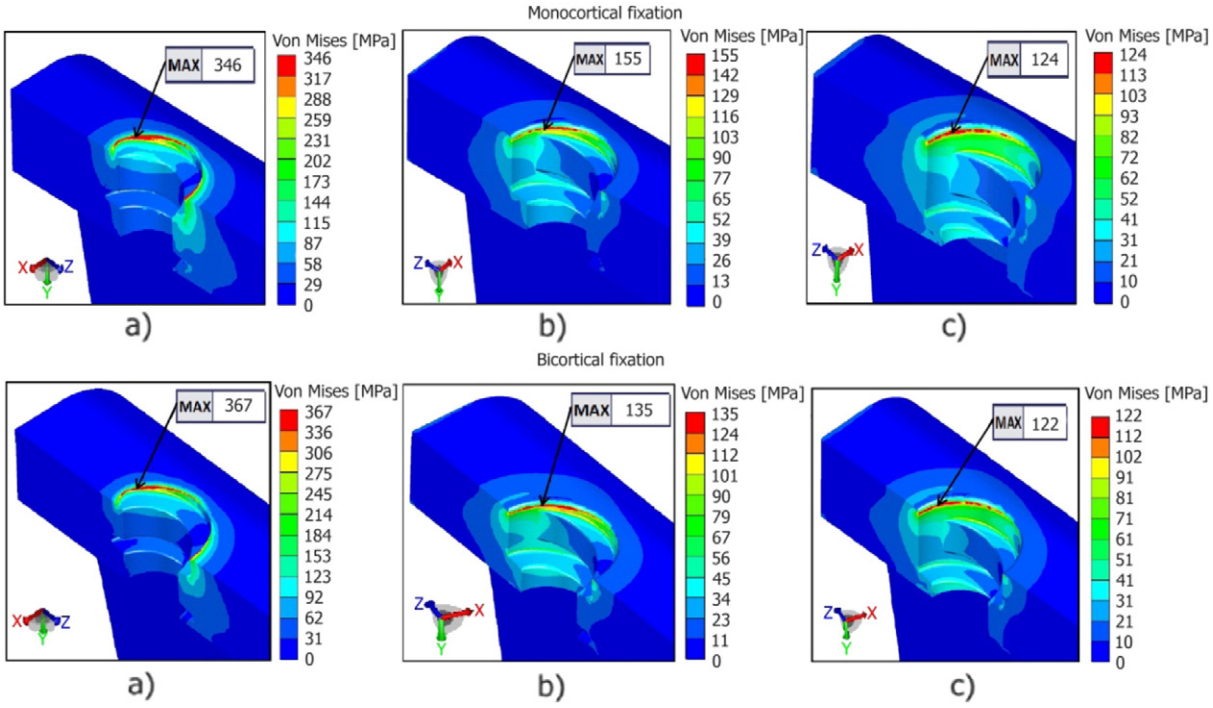

Fig. 12. The maximum stress values in the cortical bone in the case of monocortical and bicortical fixations of the implant with 14 mm intraosseal length and three positions of the thread beginning: a) 0.5 mm above, b) 0.2 mm below and c) 0.5 mm below the cortical bone surface.

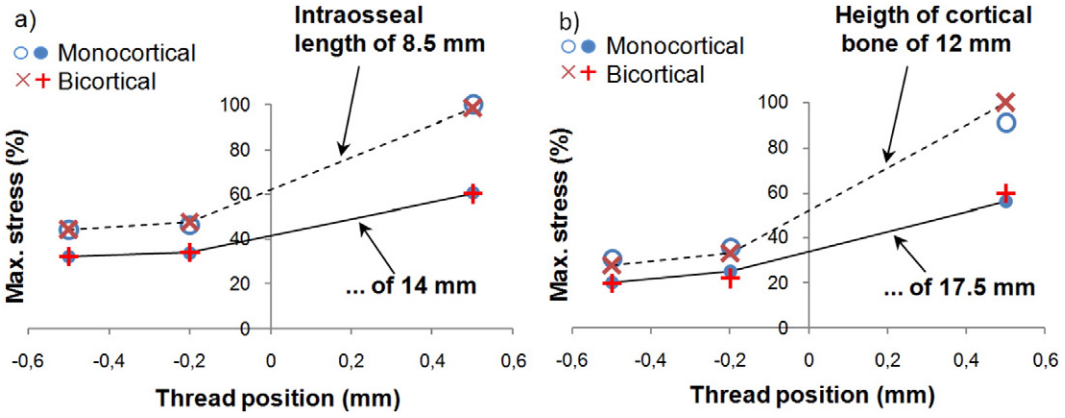

Fig. 13. Relative relationships between maximum stresses and thread positions in the case of a) implant and b) cortical bone.

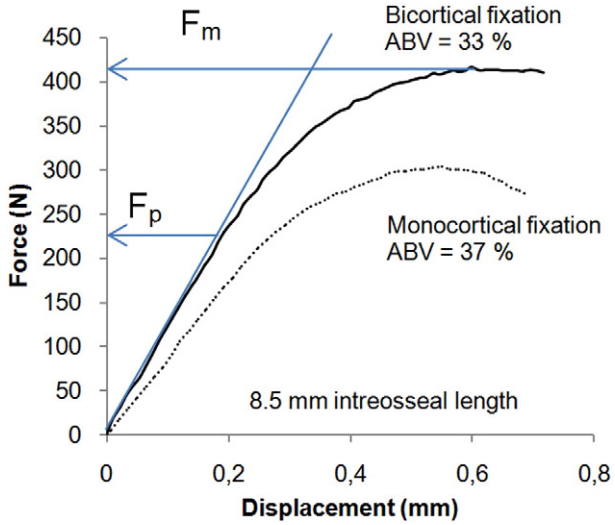

Fig. 14. The load–displacement curves from compressive tests of a model bone in an implant with mono- and bicortical fixation. The intraosseal length of the implant was 8.5 mm and the thickness of the "cortical bone" was 2.5 mm (samples no. 7 and no. 8 in Table 2).

Following simplification can be used to explain the appearance of the stress concentrator (1b). Despite relatively complex geometry of the real implants, the implant can be principally decomposed into two cylindrical segments with different diameters: one which corresponds to the extraosseal part with larger diameter and the second cylinder with smaller diameter corresponding to the intraosseal part of the implant body. The thread can be regarded as the third part of the implant which can be omitted for a while for simplicity. The analyzed 3-axial loading of the implant in the mandible can be therefore approximately described as the loading of cylindrical beam rods with different diameters inserted into a plate. The manual calculation of the maximum von Mises stress in the cylindrical beam under 3-axial loading was based on von Mises formula. It resulted in the maximum stress of 148 MPa for the extraosseal case of the rod with the diameter of 3.0 mm and "intraosseal" length of 8.5 mm. Additional FEA with the same geometry yielded the same value. This value is close to the values of 170 MPa and 190 MPa obtained in the real implant (see Table 3) screwed 0.5 mm below the bone surface in the case of bi- and monocortical fixation, respectively. When the implant thread was above the bone surface, the calculation for the cantilever beam rod with 2 mm diameter resulted in 462 MPa. The corresponding FEA values were 590 MPa and 616 MPa. Despite the difference is larger due to oversimplification of the model, the tendency is confirmed and the difference in stress is principally due to different cross section surface areas of the extraosseal implant head and intraosseal implant body at different thread positions to which the same load is applied. This approach allows us to explain not only the existence of the zone (2i) concentrator in the implant but also its shift when thread position changes with regard to bone surface (Fig. 8a vs. c and Fig. 9a vs. c) The thread position 0.5 mm above the bone surface means that zone (2i) is in the smaller diameter part of the implant and zone (1i) related to the thread root may be above the zone (2i). The situation changes to the case in Fig. 6 when the implant is screwed deeper into the

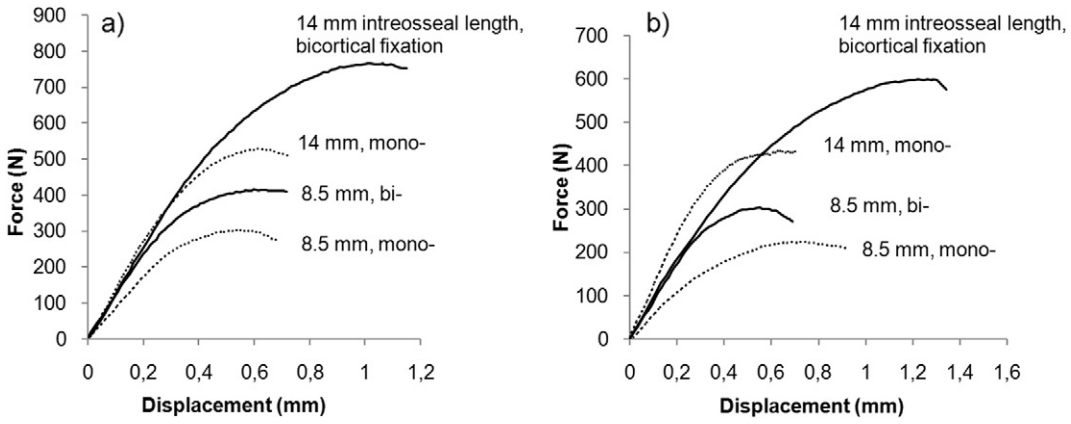

Fig. 15. The comparison of the load–displacement curves of two implants with different intraosseal lengths and different fixations in the model bone with the thickness of the ash wood (cortical bone) of 2.5 mm — a), and 2.0 mm — b).

Table 4
Average values of the load F_p at the yield strength and the load F_m at the strength limit for mono- and bicortical fixation of the implants with the intraosseal lengths of 8.5 mm and 14 mm in the model bone with two different thicknesses of the "cortical bone".

Thickness of ash wood "cortical bone"	Intraosseal length 8.5 mm		Intraosseal length 14 mm	
	"Yield" force F_p [N]	"Strength" force F_m [N]	"Yield" force F_p [N]	"Strength" force F_m [N]
Monocortical fixation				
2.0 mm	150	220	320	430
2.5 mm	250	300	410	525
Bicortical fixation				
2.0 mm	250	300	420	600
2.5 mm	340	410	550	760

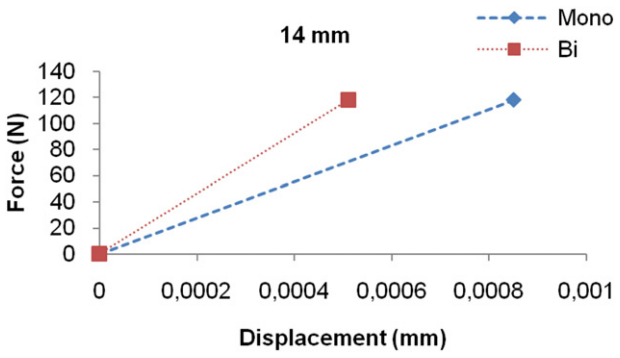

Fig. 17. The comparison of the displacements (and slopes) for the same three-axial load of 118 N obtained from FEA.

bone and significant stress reduction is obtained because of larger cross section of the extraosseal part.

The elastic deformation of the implant intentionally exaggerated in Figs. 6–7 can also be explained using the loaded cantilever beam rod model. The effect of three-axial loading would be equivalent to higher off-axial compressive loading on one side of the beam than on the other side. The result is the bending of the beam which explains the appearance of the tensile components among the principal stresses.

Stresses in the cortical bone adjacent to the implant are slightly different from those in the implant. The zone (1b) with the highest compressive stresses is located at the neck of the implant and not at the root of the thread as it is in the implant. The difference seems to be due to the fact that the edge of the bone has to resist to the bending of the implant which acts as a lever. This approach can be also used to predict possible effects of deeper screwing-in of the implant. The positions of the implant thread below the bone surface, which would correspond to the well recessed implants, generate lower stresses in the bone zone (1b) than in the position above the surface because of larger diameter and shorter lever. Because the bone atrophy shall occur in the zone with high compressive stresses, the bending load supporting edge of the bone surface may "move" from thicker head part into the thinner thread part of the implant. Subsequently, time dependent increase of the local compressive stresses in the zone (1b) can be expected as local bone atrophy occurs. Its progress is similar to unscrewing of the implant from the position "below" to the position "above" the bone surface.

All the above considerations assume that the cortical bone is the principal load-bearing part of the mandible. Indeed, the stresses in the trabecular bone were considerably smaller than in the cortical bone (see Table 4). The strong influence of the length of the intraosseal part of the implant on the maximum stress in the cortical bones with the same thicknesses in Fig. 16 is therefore surprising. Let us consider possible reasons. In the case of vertical uniaxial loading, no effect of cortical bone thickness was expected. Under multiaxial loading, trabecular bone helps to resist to the torque of the intraosseal part of the monocortical implant rotating around the axis in the upper cortical bone. Even more important seems to be that the shortening of the intraosseal part of the implant results in the increase of the extraosseal lever arm due to the constant (28.7 mm) distance from the bottom of the mandible up to the loading point at the top of the crown (see Fig. 3a). Thus, as longer is the extraosseal length as bigger is the torque and stronger the influence of implant length. It is in qualitative agreement with the data in Fig. 13. The ratio between intraosseal and extraosseal lengths should be more than 1 [24–26], otherwise multiple implants are recommended. According to Fig. 2, the corresponding ratios with the intraosseal lengths of 8.5 mm and 14 mm were 0.49–0.52 and 1.31, respectively. Evidently, the conditions in the former case are far from optimum and shortening of the intraosseal length and larger arm results in excessive torque.

The simplified model of rod-like implant fixed in the upper cortical bone allows us to understand also the differences between mono- and bicortical fixations of the implant. The principal difference of the bicortical fixation is that not only the tip of the implant fixed in the lower cortical bone takes some part of the load from the upper cortical bone but also it acts against the torque of the implant. In the case of monocortical fixation, only weak trabecular bone acts against the torque. Although FEA usually showed slightly lower stress levels in bicortical case, the differences between mono- and bicortical fixations in Fig. 13 were quite small. The real experiments indicated considerably greater differences not only in terms of F_p and F_m but also in the slope of the load–penetration depth curves (see Fig. 15a). The discrepancies in the slopes can again be rationalized within the above mentioned simplified model of the rod-like implant. The vertical displacement of the

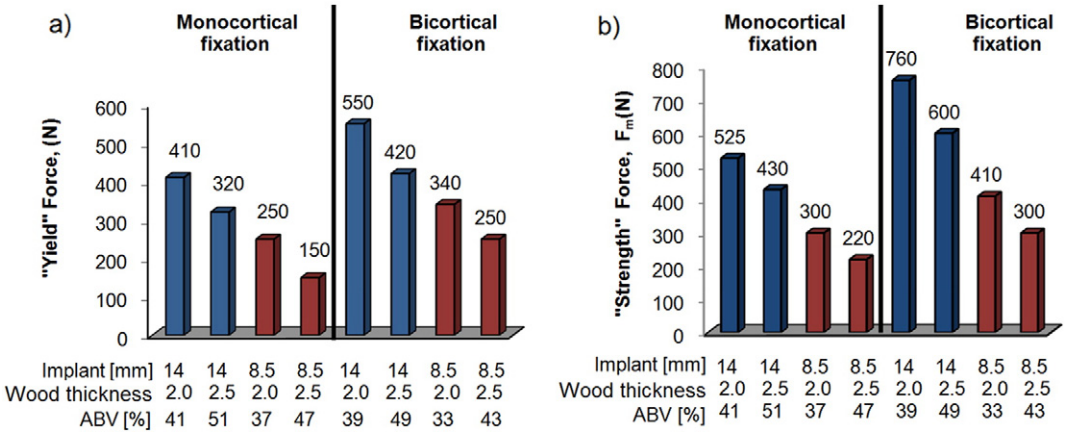

Fig. 16. a) The comparison of the force corresponding to the yield strength — a) and maximum force corresponding to the strength of the system implant/model bone — b) depending on the type of fixation, implant length, cortical bone thickness and ABV index.

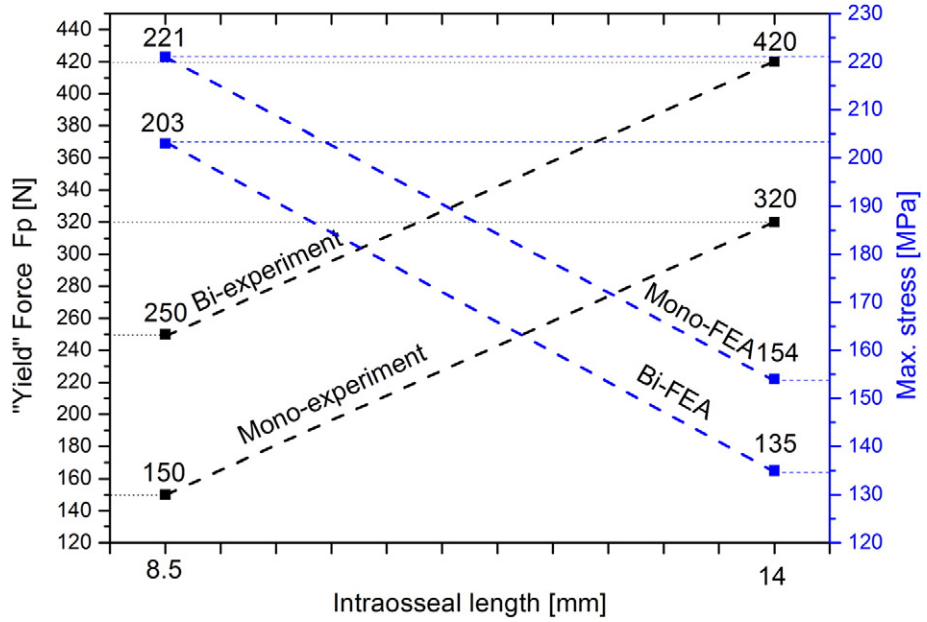

Fig. 18. The comparison of the trends from FEA and from the experimental measurements on model bone for mono- and bicortical fixations.

monocortical implant subjected to compression should be determined mainly by the elastic properties of the cortical bone because much stiffer implant only transfers the load to the bone. In contrary, the stiffness of the implant/cortical bone system in bicortical case would be controlled by the bone and much stiffer implant as well because it is indented into the lower cortical bone. The slope of the loading curve should be therefore higher than in the monocortical case. Indeed, higher slope in the bicortical case observed experimentally (Fig. 14) was confirmed also by the additional FEA for the equivalent loading (see Fig. 17). Stiffer bicortical fixation subsequently results in higher F_p and F_m experimental values than in the monocortical case. The effect of the cortical bone thickness on F_p and F_m in Fig. 16 is a direct confirmation of the earlier assumption that the upper cortical bone is bearing the main part of the load.

The understanding of the differences between FEA and experimental measurements for mono- and bicortical fixations is more complicated. The direct comparison of the maximum stresses and experimental forces is not possible because the overall forces cannot be transferred into localized stresses. However, the trends of stresses and forces for obtained from the calculations and experimental measurements should be the same. Fig. 18 compares the trends for the maximum FEA stresses and experimental "yield" forces in both fixations. The experimental data increase with intraosseal length whereas the modeled data exhibit opposite tendency. It is reasonable because the meanings of F_p and σ_{max} are different — maximum yield force has to be higher when the implant fixation is enhanced (intraosseal length is increased) while the maximum stresses have to be reduced because of the same reason. The lines connecting the corresponding data-points are parallel which means that the trends are identical in both FEA and experiment. However, the relative changes between mono- and bicortical fixation are different: they are 31–67% in the experiment but only 9–14% in the FEA. Such a large difference can hardly be related only to the variations in the elastic module of the bone and wood types. The most probable explanation is based on the consideration of the implant bonding. Strong bonding assumed in FEA cannot be achieved in the model experiment because osteointegration is absent. Thus, the experiments with the implant in model bone correspond to the freshly introduced implant while FEA describes the case with the well osteointegrated implant. This assumption has significant consequence: bicortical fixation is more efficient in the freshly introduced implant then the monocortical one but the difference is decreasing over time due to osteointegration, possibly as a result of gradual suppression of sliding between the bone and implant during loading. Thus, the differences between the model experiment and FEA as well as between mono- and bicortical fixations can be rationalized.

The final remarks justify the range of forces used for FEA and the applicability of the results in the real situation. It is obvious that the average and even maximum chewing forces applied to the implant have to be significantly lower than the yield strength forces to prevent sudden and/or fatigue bone failure with sufficient safety margin. The force of 118 N used in FEA as a reasonable upper force limit for individual teeth in the front part of the mandible [20], is at least two times lower than most of the experimentally measured forces corresponding to the yield strength (Fig. 16a). The safety margin in the case of "strength" forces of the model implant/bone system (Fig. 16b) is even higher. Only in the case of short (8.5 mm) monocortical implant in 2 mm thin cortical bone, the "yield" force of 150 N is approaching to the applied force of 118 N. Safety margin in the same bone with bicortical fixation is still more than 2. It indicates the limits of applicability of monocortical and advantage of bicortical fixation.

The current FEA and experiments correspond to the static loading which is definitely not the case during chewing. Such situation can be experimentally simulated by dynamic multi-cyclic loading. FEA of such process would require introduction of the deformation and damage mechanisms. Both cases are behind the scope of the current work. Thus, the work applies only to the case of an unrepeated bite.

5. Conclusions

The FEA of the stress distribution in the implant, cortical and trabecular bone of the atrophied mandible for the case of the implant subjected to static 3-axial loading in mono- and bicortical fixation and 3 different positions of the implant thread with regard to the cortical bone surface revealed:

- Multi-axial compressive loading generates von Mises stresses not only with compressive but also with tensile principal stresses.
- The highest compressive principal stresses in the implant are concentrated at the root of the first thread on the compressed side of the implant and in the implant neck opposite to the surface level of the cortical bone.

- The highest compressive principal stresses in the cortical bone are always generated at the edge of the cortical bone where the highest torque from the implant is acting.
- The recession of the implant thread slightly below the surface of the cortical bone is a very effective way to reduce the maximum level of compressive stresses in the implant and cortical bone as well.
- The gradual atrophy of the bone subjected to high compressive stresses at the implant neck would result in the increase of the local stresses.
- Shortening of the intraosseal length of the implant and/or thinning of the upper cortical bone result in a substantial increase of the maximum compressive stresses.
- According to FEA, bicortical fixation compared to monocortical fixation brings only small reduction of the maximum compressive stresses.

Additional model experiments using the real implant and model bone confirmed the tendencies suggested for the changes of intraosseal length and cortical bone thickness implied from FEA. However, the effects in the experiment were significantly more pronounced in bicortical fixation than in the FEA. It is because FEA describes the case of well osteointegrated implant whereas the model experiments are close to the freshly introduced implant. Apparently, bicortical fixation is the most efficient in the fresh implants and the advantage of bicortical fixation compared to monocortical fixation decreases with time due to osteointegration, possibly as a result of gradual suppression of sliding between the bone and implant during loading.

Acknowledgments

This work was supported within the frame of the projects VEGA 2/0098/14, APVV-0520-10, and NanoCEXmat II: ITMS no: 26220120035.

References

[1] P.I. Brånemark, R. Adell, U. Breine, B.O. Hansson, J. Lindstrom, A. Ohlsson, Intraosseous anchorage of dental prosthesis: I. Experimental studies, Scand. J. Plast. Reconstr. Surg. 3 (1969) 81–100.
[2] C.J. Ivanoff, K. Gröndahl, C. Berkström, U. Lekholm, P.I. Brånemark, Influence of bicortical or monocortical anchorage on maxillary implant stability: a 15-year retrospective study of Brånemark System implants, Int. J. Oral Maxillofac. Implants 15 (2000) 103–110.
[3] L. Pierrisnar, G. Hure, M. Barquins, D. Chappard, Two dental implants designed for immediate loading: a finite element analysis, Int. J. Oral Maxillofac. Implants 3 (2002) 353–362.
[4] K. Wang, D.H. Li, J.X. Zhou, C.J. Zhang, B.L. Liu, Y.L. Li, Influence of bicortical anchorage on the natural frequencies of dental implant, 1 (2006) 86–88 (Hua Xi Kou Qiang Yi Xue Za Zhi).
[5] U. Lekholm, G.A. Zarb, Patient selection and preparation, in: P.-I. Brånemark, G.A. Zarb, T. Albrektsson (Eds.), Integrated Prostheses: Osseointegration in Clinical Dentistry, Quintessence Publ Co., Chicago, 1985, pp. 199–209;
P.-I. Brånemark, U. Lelkholm, G.A. Zarb, Tissue Integrated Prostheses: Osseointegration in Clinical Dentistry, Quintessence, Chicago, 1985. 199–209.
[6] J.I. Cawood, R.A. Howell, A classification of the edentulous jaws, Int. J. Oral Maxillofac. Surg. 17 (1988) 232–236.
[7] F. Bodic, Y. Amoriq, M. Gayet-Delacroix, Y. Maugars, L. Hamel, M. Baslé, D. Chappard, Relationships between bone mass and micro-architecture at the mandible and iliac bone in edentulous subjects: a dual X-ray absorptiometry, computerised tomography and micro computed tomography study, Gerodontology 29 (2012) e585–e594.
[8] H. Eufinger, N.C. Gellrich, D. Sandmann, J. Dieckmann, Descriptive and metric classification of jaw atrophy. An evaluation of 104 mandibles and 96 maxillae of dried skulls, Int. J. Oral Maxillofac. Surg. 1 (1997) 23–28.
[9] D. Garbaccio, The Garbaccio bicortical self-threading screw, Riv. Odontosmatol. Implantoprotesi 1 (1983) 53–56.
[10] D.W. Lee, K.H. Park, I.S. Moon, The effects of off-axial loading on periimplant marginal bone loss in a single implant, J. Prosthet. Dent. (2014), http://dx.doi.org/10.1016/j.prosdent.2014.02.004.
[11] L. Barbier, E. Schepers, Adaptive bone remodeling around oral implants under axial and nonaxial loading conditions in the dog mandible, Int. J. Oral Maxillofac. Implants 12 (1997) 215–223.
[12] B.R. Ranger, R.M. Sullivan, T.M. Jemt, Load factor control for implants in the posterior partially edentulous segment, Int. J. Oral Maxillofac. Implants 12 (1997) 360–370.
[13] E.J. Richter, In vivo horizontal bending moments on implants, Int. J. Oral Maxillofac. Implants 13 (1998) 232–244.
[14] O.C. Zienkiewicz, D.W. Kelly, Finite elements — a unified problem-solving and information transfer method, Finite Elements in Biomechanics, Ed, John Wiley & Sons, Ltd., New York, 1982.
[15] A. Sertgoz, S. Guvener, Finite element analysis of the effect of cantilever and implant length on stress distribution in an implant-supported fixed prosthesis, J. Prosthet. Dent. 76 (1996) 165–169.
[16] L. Pierrisnar, F. Renouard, P. Renault, M. Barquins, Influence of implant length and bicortical anchorage on implant stress distribution, Clin. Implant. Dent. Relat. Res. 4 (2003) 254–262.
[17] J. Strecha, R. Jurkovic, T. Siebert, S. Bartáková, Fixed bicortical screw and blade implants as a non-standard solution to an edentulous (toothless) mandible, Int. J. Oral Sci. (2010) 105–110.
[18] J. Nissan, O. Ghelfan, O. Gross, I. Priel, M. Gross, G. Chaushu, The effect of crown/implant ratio and crown height space on stress distribution in unsplinted implant supporting restorations, J. Oral Maxillofac. Surg. 69 (2011) 1934–1939.
[19] D. Schneider, L. Witt, C.H. Hammerle, Influence of the crown-to-implant length ratio on the clinical performance of implants supporting single crown restorations: a cross-sectional retrospective 5-year investigation, Clin. Oral. Implants Res. 23 (2012) 169–174.
[20] R. Mericske-Stern, M. Piotti, G. Sirtes, 3-D in vivo force measurements on mandibular implants supporting overdentures: a comparative study, Clin. Oral. Implants Res. 4 (1996) 387–396.
[21] H. Van Oosterwyck, J. Duyck, J. Vander Slote, G. Van der Perre, M. De Cooman, S. Lievens, R. Puers, I. Naert, The influence of bone mechanical properties and implant fixation upon bone loading around oral implants, Clin. Oral Implants Res. 6 (1998) 407–418.
[22] J. Dvořák, V. Hrubý, J. Kadlec, M. Pospíchal, E. Svoboda, A. Martikáň, H. Konečná, I. Sedlák, The system of testing of metal dental implants, Final Report (in Czech: Systém zkoušek kovového dentálního implantátu. Závěrečná zpráva), Akademie o.p.s., Brno, 2009.
[23] R.v. Mises, Mechanik der festen Körper im plastisch deformablen Zustand, Nachr. D Kgl. Ges. Wiss. Göttingen, Math.-Phys. 4 (1913) 582–592.
[24] S.P. Sun, I.S. Moon, K.H. Park, D.W. Lee, Effect of crown to implant ratio and anatomical crown length on clinical conditions in a single implant: a retrospective cohort study, Clin. Implant. Dent. Relat. Res. (2013), http://dx.doi.org/10.1111/cid.12175.
[25] G. Telleman, G.M. Raghoebar, A. Vissnik, L. den Hartog, J.J. Huddelston Slater, H.J. Meijer, A systematic review of the prognosis of short (<10 mm) dental implants placed in the partially edentulous patient, J. Clin. Periodontol. 38 (2011) 667–676.
[26] S. Annibali, M.P. Cristalli, D. Dell'Aquila, I. Bignozzi, G. La Monaca, A. Pilloni, Short dental implants: a systematic review, J. Dent. Res. 91 (2012) 25–32.